Supplementary Materials and Methods

S1 Expanded Geologic and Paleogeographic Information

The carbonate nodules from Montañez et al., (2007) utilized in this study were collected from well-developed and drained paleosols from: 1) the Eastern Shelf of the Midland Basin (N.C. Texas), 2) Paradox Basin (S.E. Utah), 3) Pedregosa Basin (S.C. New Mexico), 4) Anadarko Basin (S.C. Oklahoma), and 5) the Grand Canyon Embayment (N.C. Arizona) (Fig. 1a; Richey et al., (2020)). The plant cuticle fossils come from localities in: 1) N.C. Texas (Lower Pease River [LPR], Lake Kemp Dam [LKD], Parkey's Oil Patch [POP], and Mitchell Creek [MC]; all representing localities that also provided carbonate nodules or plant organic matter [POM] for Montañez et al., (2007), 2) N.C. New Mexico (Kinney Brick Quarry [KB]), 3) S.E. Kansas (Hamilton Quarry [HQ]), 4) S.E. Illinois (Lake Sara Limestone [LSL]), and 5) S.W. Indiana (sub-Minshall [SM]) (Fig. 1a, S2–4; Richey et al., (2020)). These localities span a wide portion of the western equatorial portion of Euramerica during the latest Pennsylvanian through middle Permian (Fig. 1b).

S2 Biostratigraphic Correlations and Age Model

N.C. Texas stratigraphy and the position of pedogenic carbonate samples from Montañez et al., (2007) and cuticle were inferred from N.C. Texas conodont biostratigraphy and its relation to Permian global conodont biostratigraphy (Tabor and Montañez, 2004; Wardlaw, 2005; Henderson, 2018). The specific correlations used are (C. Henderson, personal communication, August 2019): (1) The Stockwether Limestone Member of the Pueblo Formation contains *Idiognathodus isolatus*, indicating that the Carboniferous-Permian boundary (298.9 Ma) and base of the Asselian resides in the Stockwether Limestone (Wardlaw, 2005). (2) The Gouldbusk Limestone Member of the Moran Formation contains a conodont that is likely in the *I. whitei* zone. This conodont is also found in the Neva Limestone of Kansas and indicates a mid- to late Asselian age (~295 Ma; Wardlaw, (2005)). (3) The Santa Anna Branch Shale and Coleman Junction Formations of the Cisco Gp contain *Sweetognathus merrilli*, indicating that these two formations span the range of occurrence of *S. merrillli* of 297.2–298.9 Ma (Wardlaw, 2005; Henderson, 2018). (4) The Hords Creek Limestone and Elm Creek Limestone Members of the Admiral and Elm Creek Formations, respectively, contain *S.* (*Rabeignathus*) *bucaramangus*, indicating an age range of 294.2–293.5 Ma (Wardlaw, 2005; Henderson, 2018). Specifically, the Elm Creek Limestone contains the top of the *S.*

(*Rabeignathus*) *bucaramangus* biozone indicating an age of 293.5 Ma and the likely position of the Asselian-Sakmarian boundary (C. Henderson, Pers. Comm. 2019). (5) The Talpa Formation in the Albany Group contains abundant brachiopods and the fusulinid taxon *Schwagerina crassitectoria*, indicating a likely Kungarian age.

Building upon this information, the plant and paleosol localities used in Montañez et al., (2007) were assigned ages using these N.C. Texas biostratigraphic correlations, previous stratigraphic reconstructions (Tabor and Montañez, 2004; Montañez et al., 2007), the ages for bracketing stages from the most recent geologic timescale (Ogg et al., 2016), and interpolating ages between age-constraints using long-term sedimentation rates (Richey et al., 2020).

Age uncertainties for localities (Richey et al., 2020) account for both stratigraphic resolution and bracketing geochronologic control, the latter a function of the age uncertainties for the latest Carboniferous and early Permian as reported in the geologic timescales (Gradstein et al., 2012; Ogg et al., 2016). Chronostratigraphic assignments for the earliest Permian deposits are extrapolated into the US midcontinent from a high-precision U-Pb calibrated succession in the Urals (Russia) using the conodonts *S. merrilli* and *S. Bucaramangus* (298.9–293.8 Ma) and *S. crassitectoria* (293.4–290 Ma; Eros et al., (2012); Schmitz and Davydov, (2012)). Reported analytical uncertainties for the U-Pb ages were propagated from the bracketing samples and used to assign temporal uncertainty to the pCO_2 curve (Richey et al., 2020). For the middle Permian Clear Fork Group, age constraints and uncertainties are based on the Leonardian-Guadalupian Boundary (272.3 Ma) and extrapolated from the closest high precision ages in the Capitanian (Gradstein et al., 2012; Ogg et al., 2016). The stratigraphic uncertainties are assigned based on depositional setting: 1) ± 100 Kyr for the channel sandstones, 2) ± 1 Myr for restricted shallow-water limestones, and 3) ± 4 Myr for paleosol-hosting, red mudstones and siltstones (Richey et al., 2020).

S3 Paleosol Carbonate-Based pCO_2 Estimates

S3.1 Model

pCO_2 estimates from Montañez et al., (2007) were generated using the carbonate CO_2 paleobarometer (Cerling, 1992):

$$CO_{2(atm)} = S_{(z)} \cdot \frac{\delta^{13}C_s - (1.0044 \cdot \delta^{13}C_r) - 4.4}{\delta^{13}C_a - \delta^{13}C_s} \quad \text{(Eq. S1)}$$

where $S_{(z)}$ is the concentration of soil-respired CO_2, $\delta^{13}C_S$ is the carbon isotopic composition of soil CO_2 (inferred from the $\delta^{13}C$ of pedogenic calcite [$\delta^{13}C_{Calc}$]), $\delta^{13}C_r$ is the carbon isotopic composition of soil-respired CO_2 (inferred from the $\delta^{13}C$ of

time-equivalent organic matter [$\delta^{13}C_{OM}$]), and $\delta^{13}C_a$ is the carbon isotopic composition of atmospheric CO_2 (inferred from the $\delta^{13}C$ of time-equivalent marine carbonate [$\delta^{13}C_{Carb}$]).

In this study, we utilized a newer MATLAB model, the Paleosol Barometer Uncertainty Quantification model (PBUQ; Breecker, (2013)). PBUQ builds upon the original carbonate CO_2 paleobarometer (Eq. S1) by allowing the user to choose from all the most recently defined methods to calculate $S_{(z)}$, $\delta^{13}C_S$, $\delta^{13}C_r$, and MAT (used, along with the $\delta^{13}C_{Calc}$, to calculate $\delta^{13}C_a$ (Romanek et al., 1992)). PBUQ improves atmospheric CO_2 estimates by utilizing a Monte Carlo approach to fully propagate uncertainty in all input parameters, producing 10,000 CO_2 estimates from which the mean, median, and 16^{th} and 84^{th} percentile error estimates are generated (Breecker, 2013).

In the methods and this supplemental document, a full account is given of the input parameters used in the PBUQ model in this study and how those input parameters differ from Montañez et al., (2007). All other data and input parameters not presented here are unchanged from Montañez et al., (2007).

S3.2 $S_{(z)}$

Among paleosol barometer variables, $S_{(z)}$ represents the most significant uncertainty due to the lack of estimates of $S_{(z)}$ in modern soils (Montañez, 2013). $S_{(z)}$ was originally assigned values based on broad environmental interpretations (i.e., paleosols formed in deserts vs. temperate or tropical environments) or assigned a single constant value (5000 ppm) (Brook et al., 1983; Cerling, 1992). Montañez et al., (2007) improved upon these methods by inferring ranges of $S_{(z)}$ values via comparison of the morphology of fossil paleosols and modern analog soils. That approach subsequently improved further via analysis of $\delta^{13}C_{Carb}$ and $\delta^{13}C_{OM}$ in Holocene soils, defining a range of $S_{(z)}$ values for modern soils (Montañez, 2013). In this study, we utilize the latter option from Montañez, (2013).

S3.3 $\delta^{13}C_r$ (Inferred from $\delta^{13}C_{OM}$)

Montañez et al., (2007) used the $\delta^{13}C$ of well-preserved plant fossil organic matter ($\delta^{13}C_{POM}$) from adjacent and roughly time-equivalent sediments as a proxy for $\delta^{13}C_r$. However, it is suggested that the use of plant organic matter can result in anomalously high pCO_2 estimates (Myers et al., 2012) and that the $\delta^{13}C$ of organic matter occluded within the targeted

carbonate nodules ($\delta^{13}C_{OOM}$) better estimates $\delta^{13}C_r$ (Myers et al., 2016), despite the possibility of post-deposition microbially-mediated alteration (Wynn, 2007). Because of this, in this study, we utilize $\delta^{13}C_{OOM}$ as a proxy of $\delta^{13}C_r$ (Richey et al., 2020).

Carbonate nodules remaining from the analysis by Montañez et al., (2007) were powdered in a shatterbox and approximately six grams of calcite were dissolved in 10% HCl. Decarbonated sediments where vacuum filtered on cellulose nitrate filter paper. Approximately 250 mg of de-carbonated sediment was analyzed at the Stable Isotope Facility, University of California, Davis. Notably, ~250 mg (the maximum amount that can be analyzed at the Stable Isotope Facility) was necessary to produce the required 100 µg of carbon for isotopic analysis due to the low organic carbon content in pedogenic carbonate nodules (range all samples ~.03–0.36% organic carbon).

A boxplot of $\delta^{13}C_{POM}$ vs. $\delta^{13}C_{OOM}$ shows that $\delta^{13}C_{OOM}$ is 3‰ more negative than $\delta^{13}C_{POM}$ with no overlap of error envelops, indicating that $\delta^{13}C_{POM}$ and $\delta^{13}C_{OOM}$ are significantly different (Fig. S5). We attribute the difference in isotopes to OOM samples that come directly from paleosol carbonate nodules, representing the same early glacial portion of a glacial cycle, in contrast to plant organics, which are typically deposited in younger glacial mudstones. This indicates a temporal separation of the two organic matter types of up to 10^4 yr.

Use of $\delta^{13}C_{OOM}$ increased pCO_2 estimates of ~30–100%, with the greatest change occurring at lower CO_2 levels. Notably, the use of $\delta^{13}C_{OOM}$ resulted in fewer biologically untenable CO_2 estimates (i.e., two < 170 ppm, the level at which plants begin to be severely affected by RuBisCo limitation due to CO_2 starvation (Ward et al., 2005; Gerhart and Ward, 2010) than the use of $\delta^{13}C_{POM}$ (15 < 170 ppm). We take this result as further evidence for $\delta^{13}C_{OOM}$ being a more appropriate proxy for $\delta^{13}C_r$.

S3.4 $\delta^{13}C_a$ (Inferred from $\delta^{13}C_{Carb}$)

Montañez et al., (2007) calculated $\delta^{13}C_a$ from the $\delta^{13}C$ value of contemporaneous brachiopods (Grossman et al., 2008) and the equation that describes the temperature-sensitive fractionation between marine calcite and atmospheric CO_2 (Romanek et al., 1992):

$$\varepsilon_{\text{calcite}-CO2} = 11.98(\pm 0.13) - 0.12(\pm 0.01) \cdot T(℃) \quad \text{(Eq. S2).}$$

However, the shallow marine brachiopods used in Grossman et al., (2008) increase the possibility of post-depositional alteration of the $\delta^{13}C$ signal. Instead, we utilize a recent compilation of deep-marine carbonate $\delta^{13}C$ (Naqing succession, Dian-Qian-Gui Sea, China) because they show no evidence of sub-areal exposure, mitigating the possibility of post-depositional alteration (Buggisch et al., 2011). These data and contemporaneous estimates of mean annual temperature (MAT; Tabor and Montañez, (2005); Tabor et al., (2013)) were used in the Eq. S2 (Romanek et al., 1992) by PBUQ to estimate $\delta^{13}C_a$ (Richey et al., 2020).

To accomplish this, the ages from Buggisch et al., (2011) were updated to reflect the most recent geologic timescale (Ogg et al., 2016). Within the updated time series, if an individual $\delta^{13}C_{Carb}$ value occurred within 10 kyr of the age of an individual paleosol, that value was used directly with an error of 0.2‰ (i.e., four times the error of $\delta^{13}C_{Carb}$ reported in Buggisch et al., (2011)). If such a value was not available, the two closest $\delta^{13}C_{Carb}$ values were averaged and used with an error of 0.4‰ to account for the uncertainty in this method (Richey et al., 2020).

To check the validity of using the data from Buggisch et al., (2011), PBUQ was also run using a more recent $\delta^{13}C_{Carb}$ compilation (Chen et al., 2018), featuring data from both Grossman et al., (2008) and Buggisch et al., (2011). CO_2 estimates from that model run did not significantly vary from runs using data from Buggisch et al., (2011), resulting in a change in CO_2 of 10s of ppm (range = ~1 to 80 ppm, with 85% of the data showing a change of <10 ppm). Due to this, we continued to use data from Buggisch et al., (2011).

S3.5 Changes to the PBUQ Model Code

PBUQ model runs conducted in this study resulted in several biologically untenable CO_2 estimates for some localities (i.e., ≤170 ppm; Gerhart and Ward, (2010)). To limit estimates below that threshold, two changes to the PBUQ Matlab code were applied:

1) In the `soil_derived_component_of_soil_CO2` file,

```
for j = 1:m-1
            if soilorder(j) == 1
                bestSz(j) = median(Mollisol_Sz);
            elseif soilorder(j) == 2
                bestSz(j) = median(Alfisol_Sz);
            elseif soilorder(j) == 3
```

```
                bestSz(j) = median(Aridisol_Sz);
            elseif soilorder(j) == 4
                bestSz(j) = median(Vertisol_Sz);
            elseif soilorder(j) == 5
                bestSz(j) = median(Andisol_Sz);
            elseif soilorder(j) == 6
                bestSz(j) = median(Inceptisol_Sz);
            end
```

(lines 460-473) were altered to

```
for j = 1:m-1
            if soilorder(j) == 1
                bestSz(j) = trimmean(Mollisol_Sz,25);
            elseif soilorder(j) == 2
                bestSz(j) = trimmean(Alfisol_Sz,25);
            elseif soilorder(j) == 3
                bestSz(j) = trimmean(Aridisol_Sz,25);
            elseif soilorder(j) == 4
                bestSz(j) = trimmean(Vertisol_Sz,25);
            elseif soilorder(j) == 5
                bestSz(j) = trimmean(Andisol_Sz,25);
            elseif soilorder(j) == 6
                bestSz(j) = trimmean(Inceptisol_Sz,25);
             end.
```

and

2) In the `monte_carlo_error_prop` file,

```
atm_CO2_estimate (1,:) = median(Ca)
```

(line 693) was altered to

```
atm_CO2_estimate (1,:) = trimmean(Ca, 25).
```

Code alteration one trimmed the means of the range of $S_{(z)}$ values used in the model by 25%. Likewise, code alteration two trimmed the ranges of values for each atmospheric CO_2 estimate by the model by 25%. A sensitivity analysis was performed using the following combinations: 1) trimmed $S_{(z)}$ means; untrimmed Monte Carlo estimates and 2) untrimmed $S_{(z)}$ means; trimmed Monte Carlo estimates. Ultimately, combination two was found to provide the least amount of estimates below the 170 ppm threshold and was utilized in this study.

S4 Stomatal-Based CO_2 Estimates

S4.1 Plant Fossil Localities

S4.1.1 Sub-Minshall

SM is a seasonally dry flora from sediments from the defunct Brazil Coal and Clay Company, Clay County, S.W. Indiana, consisting almost exclusively of the dry-adapted plant species *Cordaites* and *Lesleya*, with rare wet-adapted elements and abundant charcoal (DiMichele et al., 2016), though a separate wet-adapted Minshall flora also exists. In this study, we utilize cuticles of the recently described species *C. minshallensis* (Šimůnek, (2018); Fig. S4a, Richey et al., (2020)).

The flora occurs in a shale stratum below the Minshall Coal and above the Upper Block Coal of the Brazil Formation. The Upper Block Coal was included in the CO_2 compilation of Montañez et al., (2016) and is assigned a revised age of 313.09 Ma in this study (Richey et al., 2020). Due to this, we assign SM an age of 312.97 Ma. Furthermore, we assign an age uncertainty of ± 0.2 Ma to represent the span of midcontinent major cyclothems (i.e., Long eccentricity, 0.4 My; Heckel, (2013); Richey et al., (2020)).

S4.1.2 Kinney Brick

KB (Tinajas Member, Atrasado Formation, central New Mexico) is a *Konservat Lagerstätte* consisting of estuarine to marine sediments preserving vertebrates, invertebrates, and plant fossils (Lucas et al., 2011). KB is a particularly important plant fossil locality, preserving ~30 species, including lycopsids, sphenopsids, ferns, pteridosperms, coniferophytes, taeniopterids, among others (DiMichele et al., 2013).

The age of KB is uncertain. Based on fossils preserved at KB, the locality was first assigned an early Permian age (Stukey, 1967). This assignment was revised to an early Virgilian age based on regional lithostratigraphy (Myers and McKay, 1976). Later, the age was updated using its stratigraphic position and biostratigraphic indicators. The best estimate of age, drawn from this evidence, is lower Missourian (middle Kasimovian) (Lucas et al., 2011). Of this evidence, the presence of the conodonts *Idiognathodus corrugatus* and *I. cherryvalensis* is significant, as it allows correlation to the *I. confragu*s zone of the North America Midcontinent region and, in turn, the Dennis cyclothem (Lucas et al., 2011; Heckel, 2013). Based on this information, we assign KB an age of 305.7 Ma (i.e., corresponding to the interglacial portion of the Dennis cyclothem) and an age uncertainty of ± 0.2 Ma to represent the span of midcontinent major cyclothems (Heckel,

(2013); Richey et al., (2020)).

Typically, KB plants are carbonized and barren of cuticle, but a small collection of macrofossils at the University of California Museum of Paleontology possesses degraded, but measurable cuticle. These cuticles were sampled, wet-mounted, and observed under UV light. Though many degraded cuticles where sampled, including walchians, cordiataleans, and peltisperms, this work produced a single viable cuticle species, identified as *Cordaites sp*. in DiMichele et al., (2013) (Fig. S4b; Richey et al., (2020)). However, recently, a new *Cordaites* species, *C. kinneyensis*, from KB was described (Šimůnek, 2018). Using the figures and description from Šimůnek, (2018), the cuticle utilized in this study was also found to be *C. kinneyensis* (Fig. S4b).

S4.1.3 Lake Sara Limestone

LSL is an informally named basal limestone of the Shumway Cyclothem, Mattoon Formation, McLeansboro Group, S.E. Illinois. LSL is found below the Shumway Limestone (part of the CO_2 reconstruction of Montañez et al., (2016) and given an updated age of 303.7 Ma in this study; Richey et al., (2020)) and above the Watson Coal, the next coal above the Calhoun Coal. The Calhoun Coal is also part of the CO_2 reconstruction of Montañez et al., (2016) and was given an updated age of ~304.13 Ma in this study (Richey et al., 2020). Given that they are part of two adjacent cyclothems, the Calhoun and Watson Coal is theoretically separated by ~400 kyr (Heckel, 2013), giving the Watson Coal an age of 303.73 Ma. Due to this evidence, we assigned LSL an age of 303.71 Ma and again assigned an age uncertainty of ± 0.2 Ma (Richey et al., 2020).

Little information is available about the LSL flora as a whole, but in this study, we utilized measurements from the recently described species *Cordaites olneyensis* (Šimůnek, (2018); Fig. S4b; Richey et al., (2020)).

S4.1.4 Hamilton Quarry

HQ, southeastern Kansas, like KB, is a *Konservat Lagerstätte* consisting of paleochannel deposits that preserve vertebrates, invertebrates, and plant fossils (Cunningham, 1993). Conifers dominate the plant assemblage, in association with sphenopsids, ferns, pteridosperms, and rare lycopsids (Cunningham, 1993). This locality is particularly rich in formally described walchian conifers (Hernandez-Castillo et al., 2001; Hernandez-Castillo et al., 2003; Rothwell et al., 2005;

Hernandez-Castillo et al., 2009a; Hernandez-Castillo et al., 2009c, b). In this study, we utilize previously prepared slides used in the formal descriptions of *Emporia royalii* (Hernandez-Castillo et al., 2009a), *E. lockardii* (Hernandez-Castillo et al., 2009c), and *E. cryptica* (Hernandez-Castillo et al., 2009b), reposited within the paleobotanical collections of the Kansas University Biodiversity Institute and Natural History Museum (Fig. S4d–f).

The age of HQ is problematic. Though the Hamilton paleochannel incised into cyclothemic sediments, inadequate exposure and the lack of overlying beds precludes the assignment of an exact age (Salley et al., 2005). However, detailed analysis and mapping of the surrounding area indicates that HQ is older than the Severy Shale but younger than the Hartford Limestone Member of the Topeka Limestone (i.e., mid-Gzhelian [mid-Virgilian]; Salley et al., (2005)). This stratigraphic evidence indicates that the most parsimonious stratigraphic position of HQ is within the Topeka cyclothem (Heckel, 2013). Thus, we assign HQ an age of 302.7 Ma (i.e., the middle of the Topeka cyclothem) and an age uncertainty of ± 0.2 Ma (Richey et al., 2020).

S4.1.5 Parkey's Oil Patch, Lake Kemp Dam, Mitchell Creek

These three localities are part of extensive plant fossil collections from the latest Pennsylvanian and through middle Permian of N.C. Texas at the National Museum of Natural History (NMNH). Each represents channel-fill deposits from fluvial to coastal plain settings. The assemblages of plants from these localities have not been formally described, but have been used to reconstruct atmospheric CO_2 via paleosols (Montañez et al., 2007), track environmental change through time (DiMichele et al., 2006), and investigate the radiation of peltasperms (DiMichele et al., 2005).

POP (uppermost Nacona Formation) cuticles were isolated from the ultimate shoots of walchian conifers and macerated. *Walchia* sp. 2 was found to be suitable to measure stomatal number and geometry and is utilized in this study (Fig. S2a; Richey et al., (2020)). LKD (basal Petrolia Formation) cuticle was isolated during exploratory palynological analysis by Carol Hotton at the NMNH. After sorting and identification at UC Davis, the LKD cuticle assemblage was found to be monotypic, consisting of a single walchian conifer morphotype, designated *Walchia* sp. 1 (Fig. S2b; Richey et al., (2020)). MC (upper Waggoner Ranch Formation) cuticle was isolated via sieving of bulk sediment, producing a diverse assemblage of 14 cuticle morphotypes. Of these, three morphotypes (a walchian conifer, voltzian conifer, and taeniopterid)

produced enough cuticles to measure stomatal parameters and are utilized in this study (Fig. S2c–e; Richey et al., (2020)). Note that the preliminary identification of MC morphotypes is based on cuticle only and awaits confirmation via linking the cuticle types to macrofossils and reproductive organs.

Because POP and MC are localities that also supplied paleosol carbonate for Montañez et al., (2007) and this study, and because LKD is time equivalent to MC, the reformulated ages, and errors of the paleosols are used for these plant localities (Richey et al., 2020).

S4.1.6 Lower Pease River

Collectively, the LPR (San Angelo and Blaine formations, Pease River Group) consists of eight plant fossil localities that track a single plant-bearing stratum across Knox, King, and Stonewall counties in N.C. Texas (DiMichele et al., 2001). In this study, we utilize material from two of these localities, Devil's Canyon and Buzzard Peak (Richey et al., 2020). LPR, like HQ, POP, LKD, and MC, represents tidal paleochannel deposits from a coastal plain environment (DiMichele et al., 2001). The LPR plant assemblage is diverse, consisting of members of the Equisetales, Coniferales, Ginkgoales, and Cycadales (DiMichele et al., 2001). Using slides that were previously prepared by Cindy Looy in order to characterize the locality and formally describe the extinct voltzian conifer *Lebowskia grandifolia* (Looy, 2007), we utilize *L. grandifolia* (Fig. S2f; Richey et al., (2020)) and three addition morphotypes (two additional voltzian conifers and taeniopterid) in this study (Figs. S3a–c; Richey et al., (2020)).

Since organic matter from Buzzard Peak was used and assigned an age in Montañez et al., (2007), we have updated the age in the manner described above for the paleosols (Richey et al., 2020). Because LPR was placed in the N.C. Texas stratigraphy using the correlation of regional strata with global stratigraphy and the ages of the base of the Capitanian and the Permian-Triassic Boundary, we used the combined error of those ages (0.5 My) as the age uncertainty of the LPR locality (Richey et al., 2020).

S4.2 Note on Walchian and Voltzian Conifers

The earliest definitive conifers in the fossil record are the walchian conifers, or walchian Voltziales (*sensu* Rothwell et

al., (2005)), a paraphyletic group of small to large trees that were prominent members of late Pennsylvanian communities in the drier areas of tropical Euramerican (Kerp et al., 1990; Rothwell et al., 1997). Walchians became ecologically important in lowland floras in the Gzhelian and Asselian (Fig. 3c; Kerp, (2000); DiMichele et al., (2006)). They were diverse, represented by several families and many genera. Walchian conifers had plagiotropic branches with helically arranged small linear to narrow triangular leaves and stomata arranged in rows or bands ((Rothwell et al., 2005; Hernandez-Castillo et al., 2009c)). In this study, we utilize walchian conifers from the HQ, POP, LKD, and MC floras (Fig. S2a–c, S4d–f).

The first definitive voltzian conifers, or voltzian Voltziales (*sensu* Rothwell et al., (2005)), are known from the Kungurian of Texas (LPR Flora, Texas; Fig. S2f; DiMichele et al., (2001); Looy, (2007); Looy and Stevenson, (2014)) and northern Italy (Forte et al., 2017) and possibly the Artinskian of Texas based on the tentative MC morphotype proposed in this study (Fig. S2e). Earlier possible occurrences in the Asselian, and possibly as far back as the Sakmarian of New Mexico, await confirmation from isolation of additional fossil material (Falcon-Lang et al., 2015; Falcon-Lang et al., 2016). The voltzian conifers are distinctly different from the walchians in the characteristics of their foliage and ovuliferous cones (or fertile cones). In contrast to walchians, the voltzians had irregular, orthotropic branching and quite variable, larger leaves which were bifacially flattened and ovate to linear, with stomata scattered or organized within rows (Clement-Westerhof, 1987; Looy, 2007). In this study, we utilize voltzian conifers from the MC and LPR floras (Figs. S2e–f, S3a, c).

S4.3 Model

Recently, Franks et al., (2014) introduced a mechanistic stomatal model for estimating paleo-CO_2 as an alternative to species-specific stomatal Index-based transfer functions. This mechanistic model uses anatomical and geochemical parameters that are readily recovered from the plant fossils as proxies for variables in the classic photosynthesis model (Farquhar et al., 1980). Stomatal size and number are used to calculate maximum stomatal conductance ($g_{c(max)}$) to CO_2, as well as operational stomatal conductance ($g_{c(op)}$ [a fraction of $g_{c(max)}$]). These data are combined with leaf boundary layer and mesophyll conductance to give total operational CO_2 conductance ($g_{c(tot)}$). Cuticle $\delta^{13}C$ values are used as a proxy for leaf $\delta^{13}C$ to estimate $\frac{C_i}{C_a}$ (the ratio of internal CO_2 to atmospheric CO_2). These data are combined with the calculated assimilation rate (A_n) to calculate atmospheric CO_2 via the following equation:

$$\text{Atmospheric } CO_2 = \frac{A_n}{g_{c(tot)} \cdot \left(1 - \frac{C_i}{C_a}\right)} \quad \text{(Eq. S3)}$$

The mechanistic model has tested favorably against ice cores (Monnin et al., 2004), traditional stomatal estimates (Kürschner et al., 1996; Richey et al., 2018), paleosol carbonate (Park and Royer, 2011)) and other proxies (GEOCARBSULFvolc; Berner, (2008)) and is considered to be an improvement over traditional stomatal proxy methods (i.e., Stomatal Index and Stomatal Density (SD; Woodward, (1987)) because the problems of species specificity (due to the ability to accurately delineate plant fossils to the species level), unknown environmental effects, and large error estimates at high CO_2 levels in the traditional methods.

S4.4 Stomatal Methods and Model Parameters

S4.4.1 Measurements of Note

Franks et al., (2014) states that if pore length (PL) can be measured directly from plant fossils, it should be used in place of guard cell length (GCL), along with a PL to GCL scaler (s1) of 1 and an error (es1) of 0 (Richey et al., 2020). PL was used for eight of the 15 morphotypes/species used in this study (Richey et al., 2020). For the remainder, no or very few stomatal pores were preserved and, as a result, GCL was used (Richey et al., 2020). However, though there were not enough pores to get a statistically significant measurement of PL for modeling, there were enough guard cells to calculate individual s1 values for most morphotypes/species, which often vary significantly from the values suggested in Franks et al., (2014) (Richey et al., 2020). In addition, for species/morphotypes were few guard cells exist, guard cell width (GCW) was estimated via GCL and the suggested GCW (pair)/GCL scaler for gymnosperms and ferns (0.6; Tables S2; Richey et al., (2020)).

Note: Šimůnek, (2018) reported SD values of *Cordaites kinneyensis* as ~110-120/mm^2 for the abaxial surface and ~70/mm^2 for the adaxial surface. Cuticles of *C. kinneyensis* measured in this study average ~65/mm^2. Using this information, and the descriptions in Šimůnek, (2018), it is likely that all cuticles isolated from University of California Museum of Paleontology specimens are all adaxial. Because of this evidence, and the close match of SD for other species calculated here and reported in Šimůnek, (2018), we have used the reported abaxial values of ~110-120/mm^2 from Šimůnek, (2018) in CO_2 modeling (Richey et al., 2020).

S4.4.2 Plant $\delta^{13}C$

The methods by which plant $\delta^{13}C$ ($\delta^{13}C_p$) was measured depended on the amount of cuticle available for analysis. For LPR, cuticle was exceedingly abundant, such that it could be sorted into morphotypes to measure morphotype-specific $\delta^{13}C_p$ values (Richey et al., 2020). LKD, POP, KB, and LSL were monotypic cuticle assemblages and, therefore, cuticle was concentrated and morphotype-specific $\delta^{13}C_p$ values were generated (Richey et al., 2020). MC cuticles were less well preserved compared to other localities. As a result, most of the cuticle was mounted on slides to measure SD and stomatal geometry and the remainder was concentrated to produce a single locality-wide plant $\delta^{13}C$ value (Richey et al., 2020).

For SM, all available cuticle of *Cordaites minshallensis* was mounted for analysis by Šimůnek, (2018). Due to this, we used the average of the $\delta^{13}C_p$ of *Cordaites* species from KB (-24.2‰) and LSL (-25.2‰) as the $\delta^{13}C_p$ value of *C. minshallensis* (-24.8‰), with the standard deviation used as an error (i.e., 0.64‰, approximately three times the analytical error of analysis by the Stable Isotope Facility, University of California, Davis; Richey et al., (2020)).

For HQ, all material was previously mounted on slides for analysis by Hernandez-Castillo et al., (2009a, b, c). However, in 2016, bulk stratigraphic sediment samples were collected at HQ and subjected to exploratory biomarker $\delta^{13}C$ analysis in the laboratory of Michael Hren (University of Connecticut). Here, we use the average n-$C_{27–31}$ *n*-alkane $\delta^{13}C$ calculated from all HQ stratigraphic samples as a substitute for cuticle $\delta^{13}C$. Studies have shown a range of isotopic offsets between compound-specific and bulk measurements (Conte et al., 2003; Diefendorf et al., 2011). In this study, we apply a 4‰ correction, the average measured fractionation of conifers (Diefendorf et al., 2015), to account for the fractionation during biosynthesis of *n*-alkanes. In addition, we use the standard deviation of all stratigraphic $\delta^{13}C$ values as the uncertainty (Richey et al., 2020).

For HQ biomarker analysis, bulk sediments were powdered in a shatterbox and freeze-dried for 24 hours. Approximately 300 g of sediment from each bulk stratigraphic sample was subjected to Soxhlet extraction in a 2:1 dichloromethane/methanol solution for 24 hours. *n*-alkanes were separated from the resulting total lipid extract via a combination of silica gel column chromatography and hexanes. Sulfur was removed from the resulting *n*-alkanes via activated copper chips. Finally, when necessary, the *n*-alkanes were further refined via urea adduction to remove contamination of branched and cyclic alkanes.

The carbon isotopic composition of n-alkanes was measured using a Thermo Scientific GC-Isolink connected to a Thermo Scientific MAT 253. Samples were injected into a split/splitless inlet at 300°C and separated on a 60 m x 20 mm x 0.25 µm DB-5 column with a He flow of 1.5 mL/min. GC oven temperature was increased from 60°C to 180°C at 12°C/min. At this temperature, the temperature was increased to 320°C at 4°C/min and held at 320°C for 10 minutes. Carbon isotopes are reported relative to VPDB and are analyzed relative to repeated measurements of an *n*-alkane isotope standard Mix A5 (Arndt Schimmelman, Indiana University, Bloomington). Repeat analyses of this standard over a range of sample sizes yield a standard deviation of 0.3‰.

Though the resulting $\delta^{13}C_p$ for HQ walchians (-24‰; Richey et al., (2020)) is more negative than the average $\delta^{13}C_p$ of other walchian conifers measured directly (i.e., -22.75 ± 0.91‰ from POP and LKD walchians), the assigned uncertainty (±1.6‰) is large enough to account for the uncertainty in both the method used to estimate $\delta^{13}C_p$ and the reported fractionation of modern conifers (Diefendorf et al., 2015).

S4.4.3 Note on $\delta^{13}C_p$

Recently, Porter et al., (2017) suggested a correction should be applied to $\delta^{13}C_p$ values used in models such as PBUQ (Breecker, 2013) and the mechanistic stomatal CO_2 model (Franks et al., 2014), especially when $\delta^{13}C_p$ is used to predict $\delta^{13}C_a$, due to the influence of phylogeny and atmospheric O_2:CO_2 ratio. However, in this study, $\delta^{13}C_a$ was independently calculated from deep-marine $\delta^{13}C_{Carb}$ (Buggisch et al., 2011) and Eq. S2 (Romanek et al., 1992)), possibly negating the need for such a correction. Furthermore, we calculated $\delta^{13}C_p$ values ranging from -22.1‰ to -25.2‰ (mean -24.04‰) and $\delta^{13}C_{POM}$ and $\delta^{13}C_{OOM}$ values ranging from -20.5‰ to -27.2 (mean -23.37‰). Using the independently inferred $\delta^{13}C_a$ values, we calculate a mean observed fractionation between $\delta^{13}C_a$ and $\delta^{13}C_p$, $\delta^{13}C_{POM}$, and $\delta^{13}C_{OOM}$ of -18.62‰, within the range of observed fractionation reported for modern gymnosperms (Arens et al., 2000; Diefendorf et al., 2010).

Nevertheless, to assess the effect, the correction for gymnosperms (-2.95‰; Porter et al., (2017)) was applied to $\delta^{13}C_p$ and the mechanistic stomatal model was rerun with those values, resulting in CO_2 increased 50–100% over those without the correction, such that values that fit comfortably within the range paleosol-based estimates (Figs. 2a, S1a) were elevated relative to the paleosol-based estimates. We interpret those results and the close match of the observed fractionation to

fractionation in modern gymnosperms as indicating that the correction is not needed in the context of this study.

S5 Late Pennsylvanian and Early Permian pCO_2 Compilation and Analysis

In this study, we present a compilation of late Pennsylvanian and early Permian pCO_2 estimates by combining estimates from this study with those of Montañez et al., (2016) (Richey et al., 2020). The carbonate nodules, rhizolith samples, and pteridosperm leaves used in Montañez et al., (2016) are from cyclothemic sediments from the Illinois Basin, U.S.A, with addition paleosols coming from the Appalachian Basin, U.S.A and the Donets Basin, Ukraine. Ages for localities used in Montañez et al., (2016) were revised and assigned uncertainties based on the stratigraphic relationship of each locality to one another and the proximity to well-dated intervals (e.g., stage boundaries; correlation to U-Pb calibrated cyclothems in the Donets Basin; Eros et al., (2012)) to reflect changes made to overlapping localities from Montañez et al. (2007) (Richey et al., 2020). Specifically, the ages from Montañez et al. (2016) were assigned uncertainties according to the following criteria: 1) localities that were closest stratigraphically to well-known and -constrained stage boundaries were assigned an error of 50 kyrs, 2) localities that occur within a 400-kyr Midcontinent cyclothem were assigned an error of 100 kyrs, 3) localities that fall within Midcontinent cyclothems whose ages are uncertain were assigned an error of 500 kyrs, and 4) localities from the Donets Basin were assigned an error of 100 kyrs (Richey et al., 2020).

Note: a few CO_2 estimates from Montañez et al. (2016) were revised during this study (Richey et al., 2020). These revised estimates do not affect the trends or interpretations presented in Montañez et al. (2016).

S6 Truncation of Age Uncertainties

The CO_2 and O_2:CO_2 age uncertainties were truncated for the LOESS analysis, constrained by the relative stratigraphic position of individual paleosols and plant fossil localities (Richey et al., 2020). Age uncertainties for adjacent localities cannot overlap because they are individual stratigraphic units separated by sediments, and, therefore, they cannot be the same age. Because of this, the individual age uncertainties were trimmed such that the errors for two adjacent samples are separated by at least 2000 years. The 2000 year separation threshold was applied because the long-term sediment accumulation rate for N.C. Texas sediments is 2–10cm/1000 yrs and each locality in the dataset is separated by at least 20

cm of sediment (minimum separation is 3 m).

Supplemental Figures

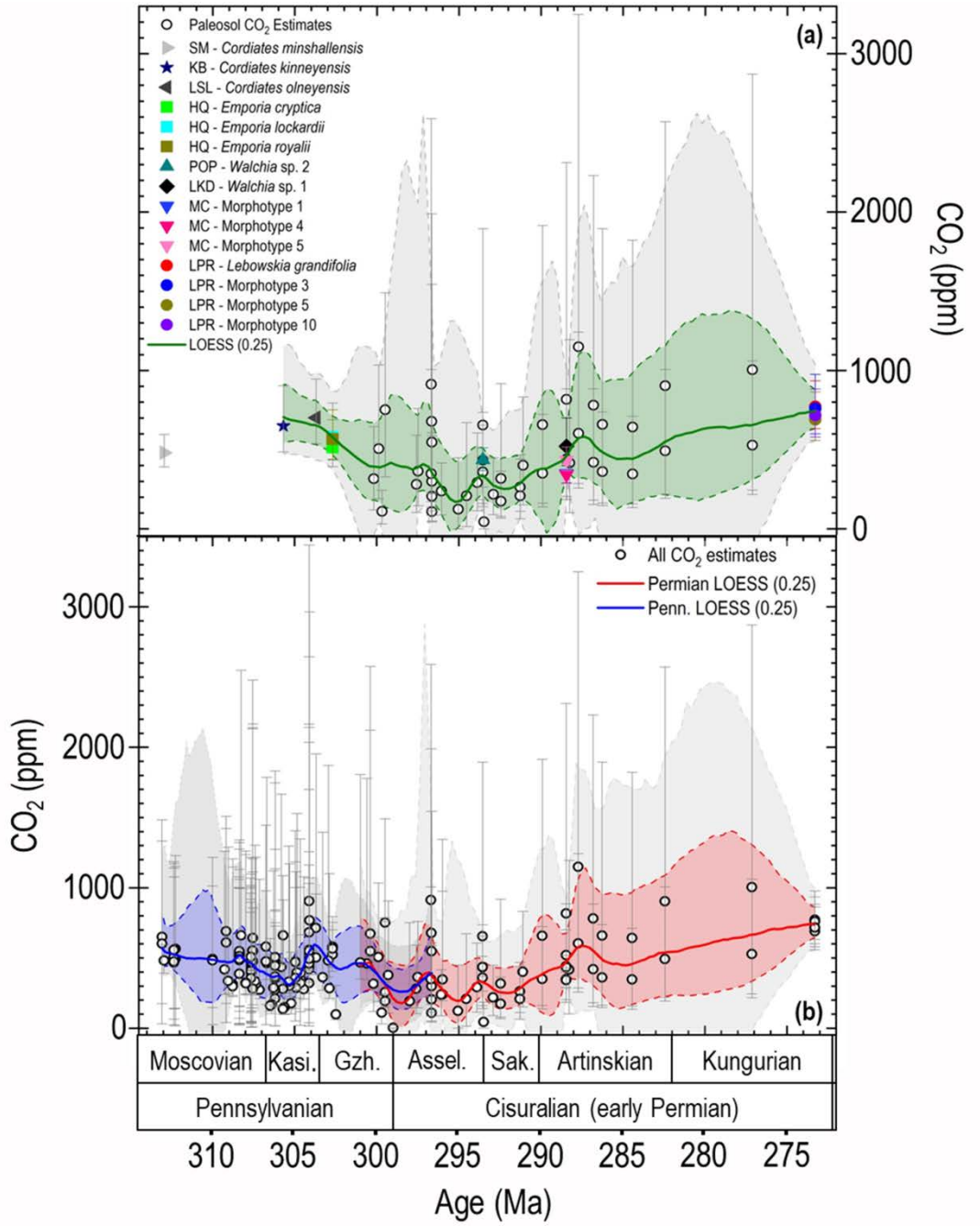

Figure S1: Comparison of the confidence intervals of LOESS analyses of this study and the Late Pennsylvanian and early Permian pCO_2 compilation and presentation of the error of individual pCO_2 estimates. (a) pCO_2 estimates from this study and LOESS analysis. Plants from SM (*Cordaites minshallensis*), KB (*C. kinneyensis*), LSL (*C. olneyensis*), HQ (*Emporia cryptica*, *E. lockardii*, *E. royalii*,), and LPR (*Lebowskia grandifolia*) that provided stomatal-based estimates are formally described (Looy, 2007; Hernandez-Castillo et al., 2009a; Hernandez-Castillo et al., 2009c, b; Šimůnek, 2018). Plants from POP (*Walchia* sp. 2), LKD (*Walchia* sp. 1), MC (morphotype 1, morph. 4, morph. 7,), LPR (morph. 3, morph. 5, morph. 10) are preliminarily described in this study. CO_2 error bars indicate the 16^{th} and 84^{th} percentiles. The gray shading is the 95% confidence interval (CI); the green shading in the 75% CI. **(b)** pCO_2 compilation (this study and Montañez et al., (2016); open circles) and LOESS analysis. The light and dark gray shading are the 95% CI; the red and blue shading in the 75% CI. Data was divided into separate Pennsylvanian and Permian curves, with significant overlap around the Pennsylvanian-Permian Boundary.

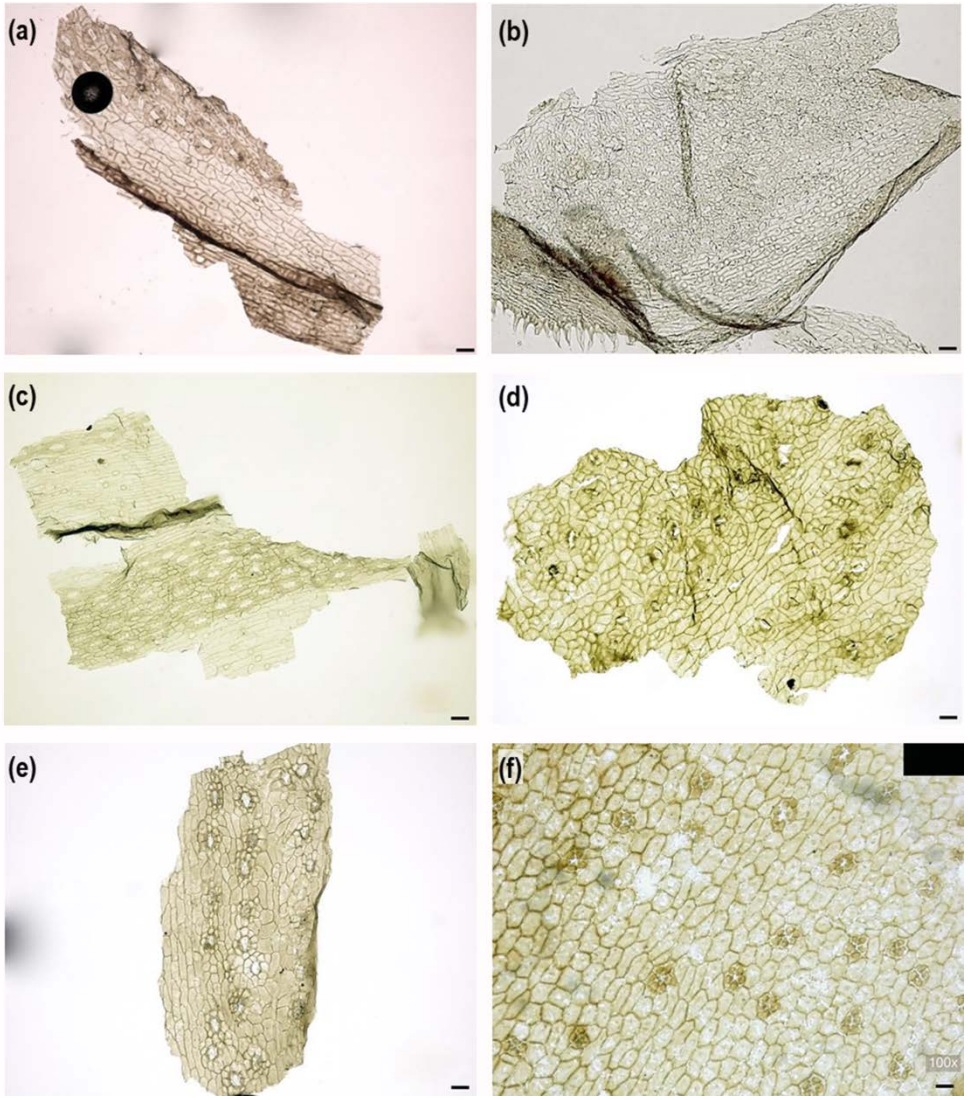

Figure S2: Permian cuticle morphotypes and species used to generate stomatal-based pCO_2 estimates. (a) *Walchia* sp. #2, POP, Smithsonian National Museum of Natural History (NMNH) specimen #USNM-528666-Wsp2-CS11-cuticle2. **(b)** *Walchia* sp. #1, LKD, NMNH specimen #USNM-40629-C. **(c)** Morphotype 4, MC, tentatively identified as a taeniopterid, NMNH specimen #USNM-32138-MC-CS25-cuticle1. **(d)** Morphotype 5, MC, tentatively identified as a voltzian conifer, NMNH specimen #USNM-32138-MC-CS5-cuticle2. **(e)** *Lebowskia grandifolia*, LPR (Looy, 2007), University of California Museum of Paleontology specimen #BP-42104-CS67-SSL1. **(f)** Morphotype 1, MC, tentatively identified as a walchian conifer, NMNH specimen #USNM-32138-MC-CS11-cuticle8 Scale for (a)–(f) 49.2 µm

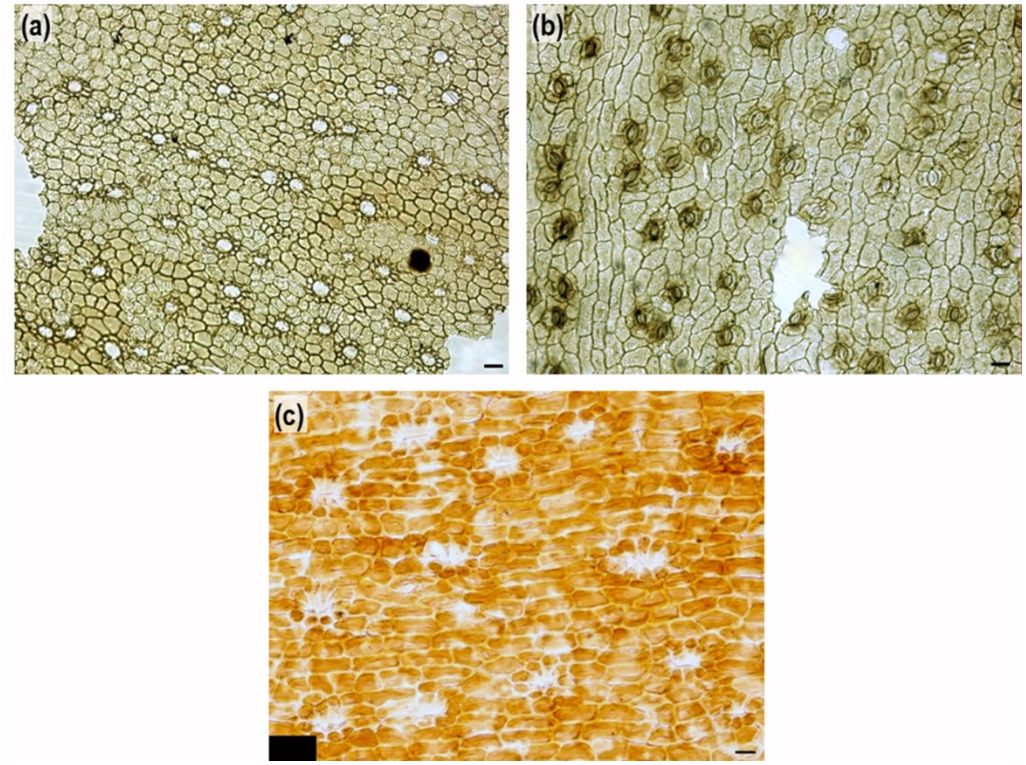

Figure S3: Additional Permian cuticle morphotypes used to generate stomatal-based pCO_2 estimates. (a) Morphotype 5, LPR, identified as a voltzian conifer, University of California Museum of Paleontology (UCMP) specimen #BP-42104-CS38. **(b)** Morphotype 10, LPR, identified as a taeniopterid, UCMP specimen #BP-42104-CS32. Scale for (a) and (b) 49.2 µm. **(c)** Morphotype 3, LPR, identified as a voltzian conifer, UCMP specimen #BP-42104-CS68-SSL2. Scale 20 µm.

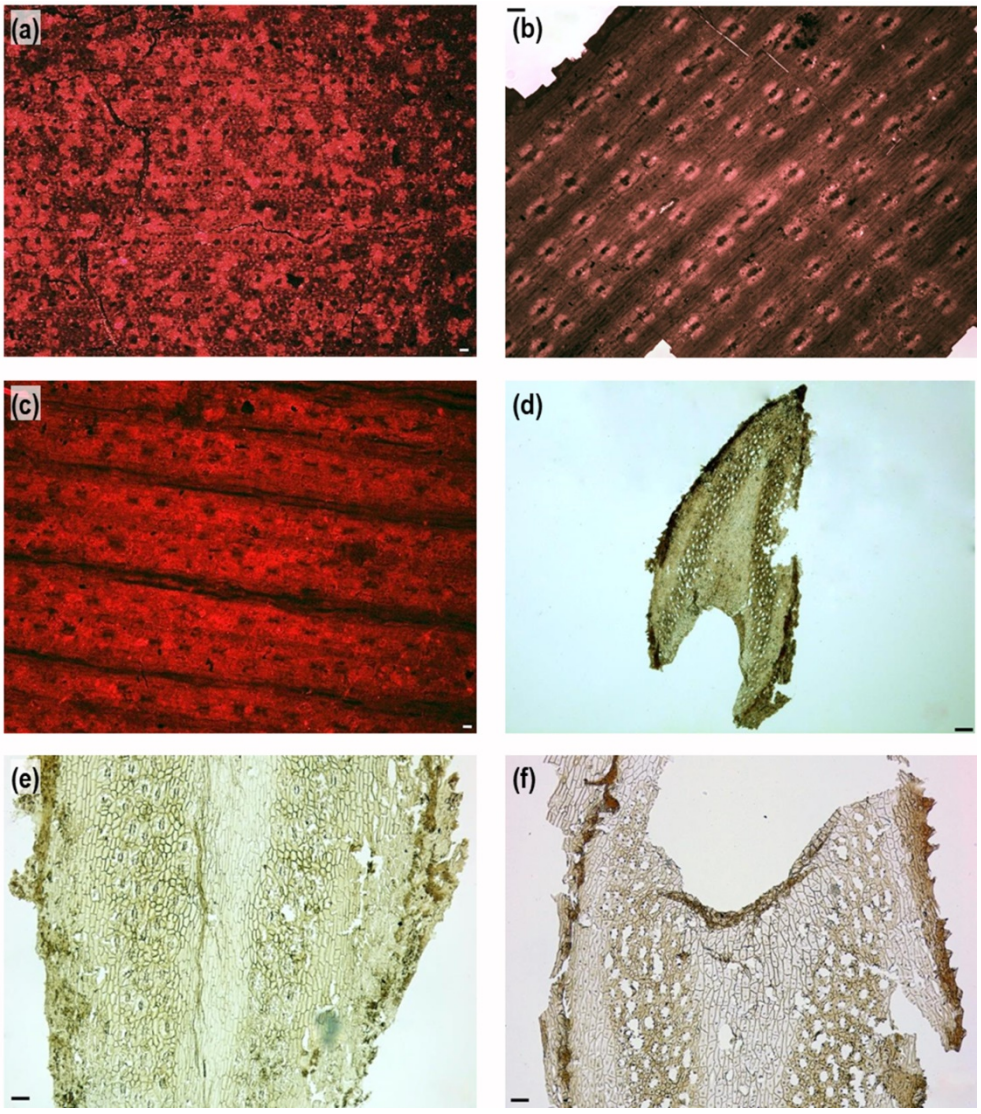

Figure S4: Pennsylvanian species used to generate stomatal-based pCO_2 estimates. **(a)** *Cordaites minshallensis*, SM (Šimůnek, 2018), Smithsonian National Museum of Natural History (NMNH) specimen #USNM-38878-RSB002A. Scale 24.6 µm. **(b)** *C. kinneyensis*, KB (DiMichele et al., 2013; Šimůnek, 2018), University of California Museum of Paleontology specimen #PA1337-UCMP200107-cuticle1. Scale 49.2 µm. **(c)** *C. olneyensis*, LSL (Šimůnek, 2018), NMNH specimen #USNM-38882-Slide6-cuticle5. Scale 24.6 µm. **(d)** *Emporia cryptica*, HQ (Hernandez-Castillo et al., 2009b), Kansas University Natural History Museum (KUNHM) specimen #KU28170. Scale 125 µm. **(e)** *E. lockardii*, HQ, KUNHM specimen #KU27968. Fig. 5a,c in Hernandez-Castillo et al., (2009c). Scale 49.2 µm. **(f)** *E. royalii*, HQ, KUNHM specimen

#KU28553. Fig. 5b, d in Hernandez-Castillo et al., (2009a). Scale 49.2 µm

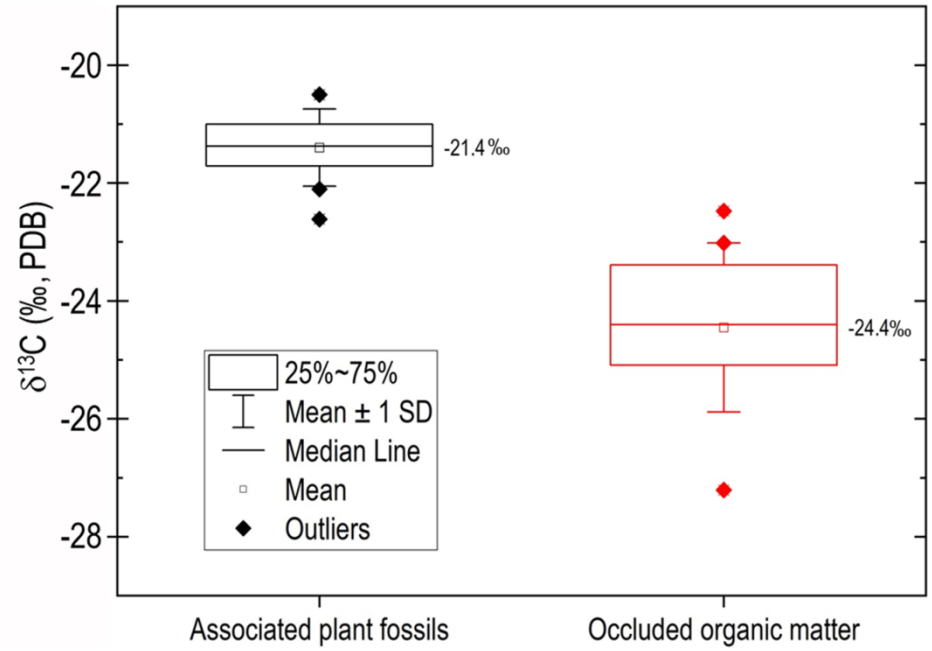

443

444 **Figure S5: Box and whisker plot of $\delta^{13}C_{OM}$ used in PBUQ (Breecker, 2013) modeling by type**.

445

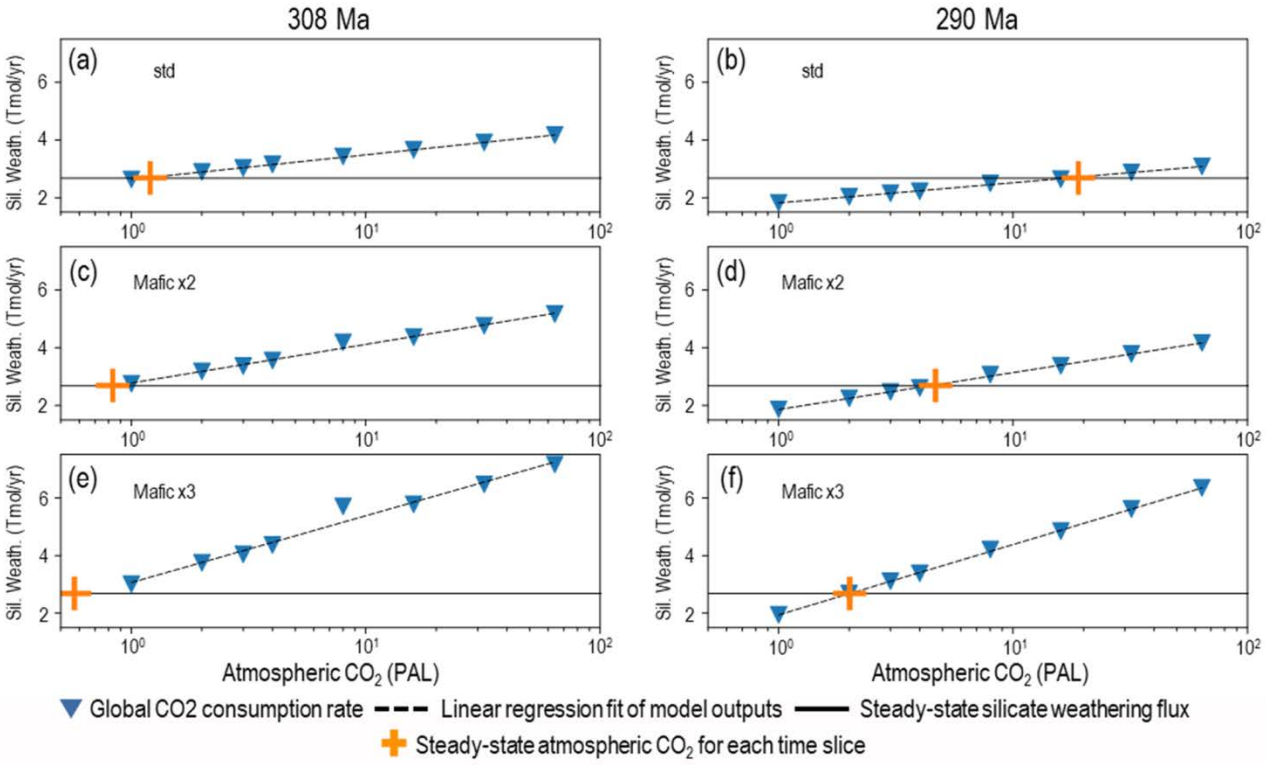

446

447 **Figure S6: Modeled global consumption rate of CO_2 through silicate weathering as a function of a range of initial**
448 **atmospheric CO_2 concentrations and varying surface area of outcropping mafic rock available for weathering**
449 **generated using the GEOCLIM model**. Global silicate weathering flux (y-axis) is calibrated to present-day global flux of
450 2.5 x 10^{12} moles of CO_2 consumed by silicate weathering (Gaillardet et al., 1999; Goddéris et al., 2017). Global CO_2
451 consumption rate (Tmoles/yr) through silicate weathering is modeled for eight initial atmospheric CO_2 concentrations
452 (logarithmic-scale relative to PAL (280 ppm)) and levels of weatherability based on simulated paleotopographic and climate
453 conditions at 308 Ma (left panels) and 290 Ma (right panels). The 'steady-state silicate weathering flux' is the level needed to
454 balance the level of solid Earth CO_2 degassing and to maintain steady-state atmospheric CO_2 above the threshold for
455 continental ice sheet initiation before the uplift of the Hercynian orogen (350 Ma; 1120 ppm (Lowry et al., 2014)). The level
456 of solid Earth CO_2 degassing, assumed to be constant between 350 to 290 Ma, is calibrated to the present-day global flux of
457 CO_2 consumed by silicate weathering and predicates that the CO_2 sink exactly balances the CO_2 source (cf. Zeebe and
458 Caldeira, (2008)). The intercept of the linear regression fit and the steady-state silicate weathering flux denotes the steady-

state atmospheric CO_2 concentration for each time slice. **(a–b)** Reference simulation using surface area of outcropping mafic rock ('std') for the late Carboniferous of Godderis et al., (2017). Results of sensitivity experiments are shown for a doubling **(c–d)** and tripling **(e–f)** of the surface area of outcropping mafic rocks. At 308 Ma (Middle Pennsylvanian and peak uplift of CPM), the steady-state atmospheric CO_2 concentration progressively shifts towards lower values staying well below the glacial threshold (840 ppm; Lowry et al., (2014)) regardless of surface area of outcropping mafic rock. A substantially higher steady-state atmospheric CO_2 concentration (3500 ppm), well above the glacial threshold for this time (560 ppm; Lowry et al., (2014)) is predicted for the reference simulation ('std'; (d)). Increasing the surface area of outcropping mafic rocks strongly impacts CO_2 concentration, which decreases to ~650 ppm for a doubling of exposed mafic rocks (e) and ~350 ppm for a tripling (f).

Supplementary Table

Table S1: Description of mechanistic model parameters

Input	Description	Method/Approximation/References
D_{ab}	Stomatal density (m^2) on abaxial surface (average over stomatal and non-stomatal areas).	Franks et al., (2014) specifies the use of leaf-wide stomatal density (SD). Due to this, most SD measurements were made at 100x to ensure that the largest area possible was measured and leaf-wide SD was approximated.
eD_{ab}	Error in D_{ab} (m^2).	Standard Error of the Mean (S.E.M.) of approximated leaf-wide stomatal density.
D_{ad}	Stomatal density (m^2) on adaxial surface (average over stomatal and non-stomatal areas).	Approximated Leaf-wide SD values used varied depending on whether individual morphotype was hypostomatic or amphistomatic.
eD_{ad}	Error in D_{ad} (m^2).	S.E.M. of leaf-wide stomatal density. Values used varied depending on whether individual morphotype was hypostomatic or amphistomatic.
GCL_{ab}	Guard cell length (m) on the abaxial surface.	Franks et al., (2014) calls for Guard Cell Length (GCL) (and a scaling factor to estimate Pore Length [PL] from GCL; PL/GCL, designated parameter s1) to be used as a model parameter, but notes that Pore Length (PL) should be used if possible (with s1 = 0). The method used for each morphotype depended on the preservation of guard cells and pores. See Supplemental Materials and Methods text for details.
$eGCL_{ab}$	Error in GCL_{ab} (m).	S.E.M. of PL or GCL (m).
GCL_{ad}	Guard cell length (m) on the adaxial surface.	PL or GCL value used varied depending on whether individual morphotype was hypostomatic or amphistomatic.

$eGCL_{ad}$	Error in GCL_{ad} (m).	S.E.M. of PL or GCL (m). Values used varied depending on whether individual morphotype was hypostomatic or amphistomatic.
GCW_{ab}	Single guard cell width (m) on the abaxial surface.	Franks et al., (2014) calls for Guard Cell Width (GCW) to be used directly, if possible. If not, Franks et al., (2014) suggests using GCL and a suggested GCW (pair)/GCL scaler for gymnosperms and ferns. The method used for each morphotype depended on the preservation of guard cells. See Supplemental Materials and Methods text for details.
$eGCW_{ab}$	Error in GCW_{ab} (m).	S.E.M. of GCW or two times the GCW error if scaled from GCL. See Supplemental Materials and Methods text for details.
GCW_{ad}	Single guard cell width (m) on the adaxial surface.	GCW or scaled GCL values used varied depending on whether individual morphotype was hypostomatic or amphistomatic.
$eGCW_{ad}$	Error in GCW_{ad} (m).	S.E.M. of GCW or two times the GCW error if scaled from GCL values used varied depending on whether individual morphotype was hypostomatic or amphistomatic.
$\delta^{13}C_p$	The ratio of 13C/12C isotopes in leaf material (PDB; ‰).	Most cuticle $\delta^{13}C$ was analyzed at the Stable Isotope Facility, University of California, Davis. For Hamilton Quarry (HQ), *n*-alkane average n-$C_{27–31}$ $\delta^{13}C$ was measured in the laboratory of Dr. Michael Hren at the University of Connecticut. For SM plants, the average $\delta^{13}C$ of other *Cordaites* species was used as insufficient material was available for analysis. See Supplemental Materials and Methods text for details.
$e\delta^{13}C_p$	Error in $\delta^{13}C_p$ (PDB; ‰).	Used UC Davis Stable Isotope Facility analytical precision of ±0.2‰ for most samples. For HQ, we used the standard deviation of the stratigraphic samples collected in 2016. For SM plants, we used the standard deviation of the $\delta^{13}C$ of other *Cordaites* species. See Supplemental Materials and Methods text for details.
$\delta^{13}C_a$	The ratio of $^{13}C/^{12}C$ isotopes in (paleo-) atmosphere air, relative to that in the PDB standard (‰).	We utilize the equation that describes the temperature-dependent enrichment of $\delta^{13}C$ in biogenic calcite (Romanek et al., 1992) and $\delta^{13}C$ values deep-marine carbonates (Buggisch et al., 2011) and contemporaneous estimates of mean annual temperature (Tabor and Montañez, 2005; Tabor et al., 2013; Montañez et al., 2016).
$e\delta^{13}C_a$	Error in $\delta^{13}C_a$.	Used suggested error of 1‰.
CO_0	Atmospheric CO_2 concentration associated with A_0 (ppm) (e.g., present-day value).	Used the present CO_2 level of 400 ppm.
A_0	The photosynthetic rate at CO_0 ($\mu mol/m^2/s$).	Franks et al., (2014) suggests the value of 10 $\mu mol/m^2/s$ for conifers and based on published measurements from extant plants. For the two taeniopterid morphotypes, we use value reported suggested for ferns and cycads (6 $\mu mol/m^2/s$).
eA_0	Error in A_0.	Used the suggested error of 1 $\mu mol/m^2/s$.
g_b	Boundary layer conductance to CO_2 ($mol/m^2/s$).	Used the suggested value of 2 $mol/m^2/s$.
eg_b	Error in g_b.	Used the suggested error of 0.1 $mol/m^2/s$.
s1	Scaling from guard cell length (GCL) to	The values used varied depending PL or GCL length was used. When PL was used directly, we used 0 as the scaler is not needed. When GCL was utilized, the

	stomatal pore length (Pl).	value of the suggested s1 for gymnosperms and ferns (0.33) or an empirically derived s1 from stomatal measurements was used.
es1	Error in s1.	The values used varied depending PL or GCL length was used. When PL was used directly used we used 0 as the scaler is not needed. When GCL was utilized, the value of the suggested es1 (0.05) was used.
s2	Scaling from single guard cell width (GCW) to stomatal depth (l).	Used the suggested value of 1.
es2	Error in s2.	Used the suggested error of 0.05.
s3	Scaling from the area of a circle with the diameter of pore length to a_{max} (maximum area of the stomatal pore).	Used the suggested value for gymnosperms and ferns of 0.5.
es3	Error in s2.	Used the suggested error of 0.025.
s4	Scaling from maximum conductance to CO_2 ($g_{c(max)}$) to operational conductance to CO_2 ($g_{c(op)}$).	Used the suggested value of 0.2.
es4	Error in s4.	Used the suggested error of 0.02.
s5	Scaling from photosynthetic rate (A) to mesophyll conductance to CO_2 (g_m).	Used the suggested generic value of 0.013.
es5	Error in s5.	Used the suggested error of 0.00065.

Table S1: Description of mechanistic model parameters as defined in Franks et al., (2014) and the methods used in this study to measure or infer values. See Richey et al., (2020) for specific values used in the mechanistic model.

References

Arens, N. C., Jahren, A. H., and Amundson, R.: Can C^3 plants faithfully record the carbon isotopic composition of atmospheric carbon dioxide?, Paleobiology, 26, 137–164, https://doi.org/10.1666/0094-8373(2000)026<0137:CCPFRT>2.0.CO;2, 2000.

Berner, R. A.: Addendum to "Inclusion of the Weathering of Volcanic Rocks in the GEOCARBSULF Model": (R. A. Berner, 2006, V. 306, p. 295–302), Am. J. Sci., 308, 100–103, https://doi.org/10.2475/01.2008.04, 2008.

Breecker, D. O.: Quantifying and understanding the uncertainty of atmospheric CO_2 concentrations determined from calcic

paleosols, Geochem. Geophys. Geosy., 14, 3210–3220, https://doi.org/10.1002/ggge.20189, 2013.

Brook, G. A., Folkoff, M. E., and Box, E. O.: A world model of soil carbon dioxide, Earth Surf. Proc. Land., 8, 79–88, https://doi.org/10.1002/esp.3290080108, 1983.

Buggisch, W., Wang, X., Alekseev, A. S., and Joachimski, M. M.: Carboniferous–Permian carbon isotope stratigraphy of successions from China (Yangtze platform), USA (Kansas) and Russia (Moscow Basin and Urals), Palaeogeogr. Palaeocl., 301, 18–38, https://doi.org/10.1016/j.palaeo.2010.12.015, 2011.

Cerling, T. E.: Use of carbon isotopes in paleosols as an indicator of the pCO_2 of the paleoatmosphere, Global Biogeochem. Cy., 6, 307–314, https://doi.org/10.1029/92GB01102, 1992.

Chen, J., Montañez, I. P., Qi, Y., Shen, S., and Wang, X.: Strontium and carbon isotopic evidence for decoupling of pCO_2 from continental weathering at the apex of the late Paleozoic glaciation, Geology, 46, 395–398, https://doi.org/10.1130/G40093.1, 2018.

Clement-Westerhof, J. A.: Aspects of Permian palaeobotany and palynology, VII. the majonicaceae, a new family of late Permian conifers, Rev. Palaeobot. Palyno., 52, 375–402, https://doi.org/10.1016/0034-6667(87)90066-2, 1987.

Conte, M. H., Weber, J. C., Carlson, P. J., and Flanagan, L. B.: Molecular and carbon isotopic composition of leaf wax in vegetation and aerosols in a northern prairie ecosystem, Oecologia, 135, 67–77, https://doi.org/10.1007/s00442-002-1157-4, 2003.

Cunningham, C. R.: Hamilton Fossil-Lagerstätte (Upper Pennsylvanian, Greenwood County, Kansas): Internal Stratigraphy and Addition to the Microfossil Assemblage, Trans. K.S. Acad. Sci., 96, 131–139, https://doi.org/10.2307/3628324, 1993.

Diefendorf, A. F., Mueller, K. E., Wing, S. L., Koch, P. L., and Freeman, K. H.: Global patterns in leaf ^{13}C discrimination and implications for studies of past and future climate, Proc. Natl. Acad. Sci. U.S.A., 107, 5738–5743, https://doi.org/10.1073/pnas.0910513107, 2010.

Diefendorf, A. F., Freeman, K. H., Wing, S. L., and Graham, H. V.: Production of *n*-alkyl lipids in living plants and implications for the geologic past, Geochim. Cosmochim. Acta, 75, 7472–7485, https://doi.org/10.1016/j.gca.2011.09.028, 2011.

Diefendorf, A. F., Leslie, A. B., and Wing, S. L.: Leaf wax composition and carbon isotopes vary among major conifer

groups, Geochim. Cosmochim. Acta, 170, 145–156, https://doi.org/10.1016/j.gca.2015.08.018, 2015.

DiMichele, W. A., Mamay, S. H., Chaney, D. S., Hook, R. W., and Nelson, W. J.: An Early Permian flora with Late Permian and Mesozoic affinities from north-central Texas, J. Paleontol., 75, 449–460, https://doi.org/10.1666/0022-3360(2001)075<0449:AEPFWL>2.0.CO;2, 2001.

DiMichele, W. A., Kerp, H., Krings, M., and Chaney, D. S.: The Permian peltasperm radiation: evidence from the southwestern United States, in: The Nonmarine Permian, edited by: Lucas, S. G., and Zeigler, K. E., New Mexico Museum of Natural History and Science Bulletin, New Mexico Museum of Natural History and Science, Albuquerque, NM, 67–79, 2005.

DiMichele, W. A., Tabor, N. J., Chaney, D. S., and Nelson, W. J.: From wetlands to wet spots: environmental tracking and the fate of Carboniferous elements in Early Permian tropical floras, in: Wetlands through time, edited by: Greb, S. F., and DiMichele, W. A., Geological Society of America Special Papers, The Geological Society of America, Boulder, CO, 223–248, 2006.

DiMichele, W. A., Wagner, R. H., Bashforth, A. R., and Álvárez-Vazquez, C.: An update on the flora of the Kinney Quarry of central New Mexico (Upper Pennsylvanian), its preservational and environmental significance, in: Carboniferous-Permian transition in central New Mexico, edited by: Lucas, S. G., Nelson, W. J., DiMichele, W. A., Speilmann, J. A., Krainer, K., Barrick, J. E., Elrick, S., and Voigt, S., New Mexico Museum of Natural History and Science, Bulletin, New Mexico Museum of Natural History and Science, Albuquerque, New Mexico, 289–325, 2013.

DiMichele, W. A., Bashforth, A. R., Eble, C. F., and Nelson, W. J.: A Middle Pennsylvanian (early Asturian) tropical dry forest, Atokan-Desmoinesian boundary, Illinois Basin, USA, Span. J. Palaeont., 31, 41–84, 2016.

Eros, J. M., Montañez, I. P., Osleger, D. A., Davydov, V. I., Nemyrovska, T. I., Poletaev, V. I., and Zhykalyak, M. V.: Sequence stratigraphy and onlap history of the Donets Basin, Ukraine: insight into Carboniferous icehouse dynamics, Palaeogeogr. Palaeocl., 313, 1–25, https://doi.org/10.1016/j.palaeo.2011.08.019, 2012.

Falcon-Lang, H. J., Lucas, S. G., Kerp, H., Krainer, K., Montañez, I. P., Vachard, D., Chaney, D. S., Elrick, S. D., Contreras, D. L., Kurzawe, F., DiMichele, W. A., and Looy, C. V.: Early Permian (Asselian) vegetation from a seasonally dry coast in western equatorial Pangea: Paleoecology and evolutionary significance, Palaeogeogr. Palaeocl., 433, 158–173,

https://doi.org/10.1016/j.palaeo.2015.05.010, 2015.

Falcon-Lang, H. J., Kurzawe, F., and Lucas, S. G.: A Late Pennsylvanian coniferopsid forest in growth position, near Socorro, New Mexico, U.S.A.: tree systematics and palaeoclimatic significance, Rev. Palaeobot. Palyno., 225, 67–83, https://doi.org/10.1016/j.revpalbo.2015.11.008, 2016.

Farquhar, G. D., von Caemmerer, S., and Berry, J. A.: A biochemical model of photosynthetic CO_2 assimilation in leaves of C3 species, Planta, 149, 78–90, https://doi.org/10.1007/BF00386231, 1980.

Forte, G., Kustatscher, E., van Konijnenburg-van Cittert, J. H. A., Looy, C. V., and Kerp, H.: Conifer diversity in the Kungurian of Europe—Evidence from dwarf-shoot morphology, Rev. Palaeobot. Palyno., 244, 308–315, https://doi.org/10.1016/j.revpalbo.2017.01.004, 2017.

Franks, P. J., Royer, D. L., Beerling, D. J., Van de Water, P. K., Cantrill, D. J., Barbour, M. M., and Berry, J. A.: New constraints on atmospheric CO_2 concentration for the Phanerozoic, Geophys. Res. Lett., 41, 4685–4694, https://doi.org/10.1002/2014GL060457, 2014.

Gaillardet, J., Dupré, B., Louvat, P., and Allègre, C. J.: Global silicate weathering and CO_2 consumption rates deduced from the chemistry of large rivers, Chem. Geol., 159, 3–30, https://doi.org/10.1016/S0009-2541(99)00031-5, 1999.

Gerhart, L. M., and Ward, J. K.: Plant responses to low [CO_2] of the past, New Phytol., 188, 674–695, https://doi.org/10.1111/j.1469-8137.2010.03441.x, 2010.

Goddéris, Y., Donnadieu, Y., Carretier, S., Aretz, M., Dera, G., Macouin, M., and Regard, V.: Onset and ending of the late Palaeozoic ice age triggered by tectonically paced rock weathering, Nat. Geosci., 10, 382–386, https://doi.org/10.1038/ngeo2931, 2017.

Gradstein, F. M., Ogg, J. G., Schmitz, M., and Ogg, G.: The Geologic Time Scale 2012, Elsevier, 2012.

Grossman, E. L., Yancey, T. E., Jones, T. E., Bruckschen, P., Chuvashov, B., Mazzullo, S. J., and Mii, H.-s.: Glaciation, aridification, and carbon sequestration in the Permo-Carboniferous: The isotopic record from low latitudes, Palaeogeogr. Palaeocl., 268, 222–233, https://doi.org/10.1016/j.palaeo.2008.03.053, 2008.

Heckel, P. H.: Pennsylvanian stratigraphy of Northern Midcontinent Shelf and biostratigraphic correlation of cyclothems, Stratigraphy, 10, 3–39, 2013.

Henderson, C. M.: Permian conodont biostratigraphy, in: The Permian timescale, edited by: Lucas, S. G., and Shen, S.-Z., Geological Society, London, Special Publications, 1, The Geological Society, London, 119–142, 2018.

Hernandez-Castillo, G. R., Rothwell, G. W., and Mapes, G. K.: Thucydiaceae fam. nov., with a review and reevaluation of Paleozoic walchian conifers, Int. J. Plant Sci., 162, 1155–1185, https://doi.org/10.1086/321920, 2001.

Hernandez-Castillo, G. R., Rothwell, G. W., Stockey, R. A., and Mapes, G. K.: Growth architecture of *Thucydia mahoningensis*, a model for primitive walchian conifer plants, Int. J. Plant Sci., 164, 443–452, https://doi.org/10.7939/R39S1KW6J, 2003.

Hernandez-Castillo, G. R., Stockey, R. A., Mapes, G. K., and Rothwell, G. W.: A new voltzialean conifer *Emporia royalii* sp. nov. (Emporiaceae) from the Hamilton Quarry, Kansas, Int. J. Plant Sci., 170, 1201–1227, https://doi.org/10.1086/605874, 2009a.

Hernandez-Castillo, G. R., Stockey, R. A., Rothwell, G. W., and Mapes, G. K.: Reconstruction of the Pennsylvanian-age walchian conifer *Emporia cryptica* sp. nov. (Emporiaceae: Voltziales), Rev. Palaeobot. Palyno., 157, 218–237, https://doi.org/10.1016/j.revpalbo.2009.05.003, 2009b.

Hernandez-Castillo, G. R., Stockey, R. A., Rothwell, G. W., and Mapes, G. K.: Reconstructing *Emporia lockardii* (Voltziales: Emporiaceae) and initial thoughts on Paleozoic conifer ecology, Int. J. Plant Sci., 170, 1056–1074, https://doi.org/10.1086/605115, 2009c.

Kerp, H.: The Modernization of Landscapes during the Late Paleozoic-Early Mesozoic, in: Phanerozoic Terrestrial Ecosystems, 2017/07/21 ed., edited by: Gastaldo, R. A., and Dimichele, W. A., The Paleontological Society Papers, Cambridge University Press, Cambridge, U.K., 79–114, 2000.

Kerp, J. H. F., Poort, R. J., Swinkels, H. A. J. M., and Verwer, R.: Aspects of Permian palaeobotany and palynology. IX. conifer-dominated Rotliegend floras from the Saar-Nahe Basin (? Late Carboniferous-early Permian; SW-Germany) with special reference to the reproductive biology of early conifers, Rev. Palaeobot. Palyno., 62, 205–248, https://doi.org/10.1016/0034-6667(90)90090-6, 1990.

Kürschner, W. M., van der Burgh, J., Visscher, H., and Dilcher, D. L.: Oak leaves as biosensors of late Neogene and early Pleistocene paleoatmospheric CO_2 concentrations, Mar. Micropaleontol., 27, 299–312, https://doi.org/10.1016/0377-

8398(95)00067-4, 1996.

Looy, C. V.: Extending the range of derived Late Paleozoic conifers: *Lebowskia* gen. nov. (Majonicaceae), Int. J. Plant Sci., 168, 957–972, https://doi.org/10.1086/518256, 2007.

Looy, C. V., and Stevenson, R. A.: Earliest Occurrence of Autorotating Seeds in Conifers: The Permian (Kungurian-Roadian) *Manifera talaris* gen. et sp. nov, Int. J. Plant Sci., 175, 841–854, https://doi.org/10.1086/676973, 2014.

Lowry, D. P., Poulsen, C. J., Horton, D. E., Torsvik, T. H., and Pollard, D.: Thresholds for Paleozoic ice sheet initiation, Geology, 42, 627–630, https://doi.org/10.1130/G35615.1, 2014.

Lucas, S. G., Allen, B. D., Krainer, K., Barrick, J., Vachard, D., Schneider, J. W., DiMichele, W. A., and Bashforth, A. R.: Precise age and biostratigraphic significance of the Kinney Brick Quarry Lagerstätte, Pennsylvanian of New Mexico, USA, Stratigraphy, 8, 7–27, https://doi.org/10.1086/518256, 2011.

Monnin, E., Steig, E. J., Siegenthaler, U., Kawamura, K., Schwander, J., Stauffer, B., Stocker, T. F., Morse, D. C., Barnola, J. M., and Bellier, B.: EPICA Dome C ice core high resolution Holocene and transition CO_2 data, 2004.

Montañez, I. P., Tabor, N. J., Niemeier, D., DiMichele, W. A., Frank, T. D., Fielding, C. R., Isbell, J. L., Birgenheier, L. P., and Rygel, M. C.: CO_2-forced climate and vegetation instability during Late Paleozoic deglaciation, Science, 315, 87–91, https://doi.org/10.1126/science.1134207, 2007.

Montañez, I. P.: Modern soil system constraints on reconstructing deep-time atmospheric CO_2, Geochim. Cosmochim. Acta, 101, 57–75, https://doi.org/10.1016/j.gca.2012.10.012, 2013.

Montañez, I. P., McElwain, J. C., Poulsen, C. J., White, J. D., Dimichele, W. A., Wilson, J. P., Griggs, G., and Hren, M. T.: Climate, pCO_2 and terrestrial carbon cycle linkages during late Palaeozoic glacial–interglacial cycles, Nat. Geosci., 9, 824–828, https://doi.org/10.1038/ngeo2822, 2016.

Myers, D. A., and McKay, E. J.: Geologic map of the north end of the Manzano Mountains, Tijeras and Sedillo quadrangles, Bernalillo County, New Mexico, US Geological Survey, 1976.

Myers, T. S., Tabor, N. J., Jacobs, L. L., and Mateus, O.: Estimating soil pCO_2 using paleosol carbonates: implications for the relationship between primary productivity and faunal richness in ancient terrestrial ecosystems, Paleobiology, 38, 585–604, https://doi.org/10.1666/11005.1, 2012.

Myers, T. S., Tabor, N. J., Jacobs, L. L., and Bussert, R.: Effects of Different Organic-Matter Sources On Estimates of Atmospheric and Soil pCO_2 Using Pedogenic Carbonate, J. Sediment. Res., 86, 800–812, https://doi.org/10.2110/jsr.2016.52, 2016.

Ogg, J. G., Ogg, G., and Gradstein, F. M.: A concise geologic time scale: 2016, Elsevier, New York, 2016.

Park, J., and Royer, D. L.: Geologic constraints on the glacial amplification of Phanerozoic climate sensitivity, Am. J. Sci., 311, 1–26, https://doi.org/10.2475/01.2011.01, 2011.

Porter, A. S., Yiotis, C., Montañez, I. P., and McElwain, J. C.: Evolutionary differences in $\Delta^{13}C$ detected between spore and seed bearing plants following exposure to a range of atmospheric O_2:CO_2 ratios; implications for paleoatmosphere reconstruction, Geochim. Cosmochim. Acta, 213, 517–533, https://doi.org/10.1016/j.gca.2017.07.007, 2017.

Richey, J. D., Upchurch, G. R., Montañez, I. P., Lomax, B. H., Suarez, M. B., Crout, N. M. J., Joeckel, R. M., Ludvigson, G. A., and Smith, J. J.: Changes in CO_2 during Ocean Anoxic Event 1d indicate similarities to other carbon cycle perturbations, Earth Planet. Sci. Lett., 491, 172–182, https://doi.org/10.1016/j.epsl.2018.03.035, 2018.

Richey, J. D., Montañez, I. P., Goddéris, Y., Looy, C. V., Griffis, N. P., and DiMichele, W. A.: Primary Data from Richey et al., 2020 (Climates Of The Past [Submitted]), https://doi.org/10.25338/B8S90Q, 2020.

Romanek, C. S., Grossman, E. L., and Morse, J. W.: Carbon isotopic fractionation in synthetic aragonite and calcite: Effects of temperature and precipitation rate, Geochim. Cosmochim. Acta, 56, 419–430, https://doi.org/10.1016/0016-7037(92)90142-6, 1992.

Rothwell, G. W., Mapes, G. K., and Mapes, R. H.: Late Paleozoic conifers of North America: structure, diversity and occurrences, Rev. Palaeobot. Palyno., 95, 95–113, https://doi.org/10.1016/S0034-6667(96)00030-9, 1997.

Rothwell, G. W., Mapes, G. K., and Hernandez-Castillo, G. R.: *Hanskerpia* gen. nov. and phylogenetic relationships among the most ancient conifers (Voltziales), Taxon, 54, 733–750, https://doi.org/10.2307/25065430, 2005.

Salley, S., Morales, M., and Sleezer, R. O.: Surficial Geology of the Hamilton Quarry Area, Greenwood County, Kansas, Lawrence, KS, 2005.

Schmitz, M. D., and Davydov, V. I.: Quantitative radiometric and biostratigraphic calibration of the Pennsylvanian–early Permian (Cisuralian) time scale and pan-Euramerican chronostratigraphic correlation, Geol. Soc. Am. Bull., 124, 549–577,

https://doi.org/10.1130/B30385.1, 2012.

Šimůnek, Z.: Cuticular analysis of new Westphalian and Stephanian Cordaites species from the USA, Rev. Palaeobot. Palyno., 253, 1–14, https://doi.org/10.1016/j.revpalbo.2018.03.001, 2018.

Stukey, A. H.: Stratigraphic Relations of Pennsylvanian-Permian Strata, Manzanita Mountains, New Mexico, Master's, University of New Mexico, 1967.

Tabor, N. J., and Montañez, I. P.: Morphology and distribution of fossil soils in the Permo-Pennsylvanian Wichita and Bowie Groups, north-central Texas, USA: implications for western equatorial Pangean palaeoclimate during icehouse–greenhouse transition, Sedimentology, 51, 851–884, https://doi.org/10.1111/j.1365-3091.2004.00655.x, 2004.

Tabor, N. J., and Montañez, I. P.: Oxygen and hydrogen isotope compositions of Permian pedogenic phyllosilicates: development of modern surface domain arrays and implications for paleotemperature reconstructions, Palaeogeogr. Palaeocl., 223, 127–146, https://doi.org/10.1016/j.palaeo.2005.04.009, 2005.

Tabor, N. J., DiMichele, W. A., Montañez, I. P., and Chaney, D. S.: Late Paleozoic continental warming of a cold tropical basin and floristic change in western Pangea, Int. J. Coal. Geol., 119, 177–186, https://doi.org/10.1016/j.coal.2013.07.009, 2013.

Ward, J. K., Harris, J. M., Cerling, T. E., Wiedenhoeft, A., Lott, M. J., Dearing, M.-D., Coltrain, J. B., and Ehleringer, J. R.: Carbon starvation in glacial trees recovered from the La Brea tar pits, southern California, Proc. Natl. Acad. Sci. U.S.A., 102, 690–694, https://doi.org/10.1073/pnas.0408315102, 2005.

Wardlaw, B. R.: Age assignment of the Pennsylvanian–Early Permian succession of north central Texas, Permophiles, 46, 21–22, 2005.

Woodward, F. I.: Stomatal numbers are sensitive to increases in CO_2 from pre-industrial levels, Nature, 327, 617–618, https://doi.org/10.1038/327617a0, 1987.

Wynn, J. G.: Carbon isotope fractionation during decomposition of organic matter in soils and paleosols: Implications for paleoecological interpretations of paleosols, Palaeogeogr. Palaeocl., 251, 437–448, https://doi.org/10.1016/j.palaeo.2007.04.009, 2007.

Zeebe, R. E., and Caldeira, K.: Close mass balance of long-term carbon fluxes from ice-core CO_2 and ocean chemistry

657 records, Nat. Geosci., 1, 312–315, https://doi.org/10.1038/ngeo185, 2008.